Finite-size effects in molecular dynamics simulations: Intermediate scattering function and velocity of sound. III. Theory and application to a model krypton fluid

J. J. Salacuse

Science and Mathematics Department, Kettering University, 1700 West Third Avenue, Flint, Michigan 48504

P. A. Egelstaff

Department of Physics, University of Guelph, Guelph, Ontario, Canada N1G 2W1

We describe a method for obtaining the intermediate scattering function $I(Q,t)$ from a computer simulation: it is an extension of our earlier calculation [Salacuse, Denton, and Egelstaff, Phys. Rev. E **53**, 2382 (1996)] for the $t \to 0$ limit. We use this approach to obtain $I(Q,t)$ for low Q and t from molecular dynamics (MD) simulations of a model krypton fluid whose atoms interact via a truncated Aziz pair potential, and the results are compared over their range of validity to $I(Q,t)$ determined by the standard MD method and also by a time expansion approach. In its range of validity our approach is much more efficient than the standard MD method; however, it covers a restricted range of t due to the movement of density fluctuations (sound waves) through the simulated fluid which produces an anomaly in the time behavior of $I(Q,t)$. By analyzing $I(Q=0,t)$ the velocity of sound in the simulation is determined, and the results compare favorably with published experimental results for the sound velocity of liquid krypton.

I. INTRODUCTION

The intermediate scattering function $I(Q,t)$ plays a significant role in describing fluid structure since it is the space transform (transform variable Q) of the Van Hove correlation function $G(r,t)$, which describes the structure of a fluid in both space (r) and time (t). It is also the frequency (ω) transform of the experimentally accessible dynamic structure factor $S(Q,\omega)$. Moreover $I(Q,t)$ can be obtained from molecular dynamics (MD) simulations; but the standard method [1] of obtaining $I(Q,t)$ from simulation data is limited by the restriction that $Q \geqslant 2\pi/L$, where L is the edge length of the simulation cube: a restriction that applies also to the calculation of the static structure factor $S(Q)=I(Q,0)$. An alternative approach to calculating $S(Q)$ and $I(Q,t)$ from simulation data was presented in a previous publication [2]: it has the advantage that both $S(Q)$ and $I(Q,t)$ can be calculated (under appropriate conditions) for all wave vector magnitudes Q, including $Q \to 0$. It was necessary that certain criteria involving the radial distribution function $g(r)$ [in the case of $S(Q)$] and the Van Hove correlation function $G(r,t)$ [in the case of $I(Q,t)$] were satisfied. Here we refer to the standard method of calculating $S(Q)$ and $I(Q,t)$ from simulation results as the "vector method," and the approach presented in Ref. [2] as the "scalar method." In a subsequent paper [3] the scalar method was applied to the calculation of $S(Q)$, and the results were compared to data obtained from calculations using the modified hypernetted chain (MHNC) integral equation. The results of the two methods agreed nicely for the states chosen. In the present work, as well as in previous publications [2,3], we are concerned only with uniform, isotropic fluids.

In this paper we apply the scalar method to the time domain, and show that it can be used to obtain short time data on $I(Q,t)$ at low values of Q. Then we determine $I(Q,t)$ for a range of Q values, including $Q=0$, from MD simulations for a dense krypton fluid. For comparison we calculate $I(Q,t)$ from simulation data using both the standard approach and the time expansion approach. The effects of sound waves limit the time interval over which the scalar method and the vector method accurately give $I(Q,t)$. We use this fact to estimate the velocity of sound in our simulated fluid and suggest a general technique of determining the velocity of sound in a simulation.

The remainder of this paper is organized as follows. In Sec. II we give the salient features of both the scalar and vector approaches to calculating $S(Q)$ and $I(Q,t)$, and the time expansion method of determining $I(Q,t)$. In Sec. III we describe the MD simulations. The results of the $I(Q,t)$ calculations are given and commented upon in Sec. IV. Then in Sec. V, we present our method of obtaining the velocity of sound in a simulation and compare our estimate with experimental results. In Sec. VI we summarize our results. We conclude the paper with two Appendixes. In Appendix A we describe the analysis required to obtain $I(Q,t)$ by both the scalar and vector methods from simulation data. In Appendix B we consider how many-body forces and the size (number of particles) of a MD simulation affect the velocity of sound.

II. METHODS OF CALCULATING $I(Q,t)$

The intermediate scattering function $I(\mathbf{Q},t)$ is related to the Van Hove function $G(\mathbf{r},t)$ by [4,5]

$$I(\mathbf{Q},t) = \int d\mathbf{r} \exp(i\mathbf{Q}\cdot\mathbf{r})[G(\mathbf{r},t)-\rho], \qquad (1)$$

where ρ is the density of the fluid and $G(\mathbf{r},t)d\mathbf{r}$ is proportional to the probability of finding a particle within a volume element $d\mathbf{r}$ at position $\mathbf{r}$ and time t, given that there was an

arbitrary reference particle at $\mathbf{r}=\mathbf{0}$ and $t=0$. $I(\mathbf{Q},t)$ is related to the experimental dynamic structure factor $S(Q,\omega)$ by [4,5]

$$S(\mathbf{Q},\omega)=\frac{1}{2\pi}\int_{-\infty}^{+\infty}dt\,\exp(i\omega t)I(\mathbf{Q},t),\qquad(2)$$

where $\hbar\mathbf{Q}$ and $\hbar\omega$ are the momentum and energy transferred in a radiation scattering experiment and $S(\mathbf{Q},\omega)$ is proportional to the scattering intensity. In terms of an equilibrium ensemble, denoted by $\langle\ \rangle$, $I(\mathbf{Q},t)$ is given as [4,5]

$$I(\mathbf{Q},t)=\frac{1}{N}\left\langle\sum_{j=1}^{N}\sum_{k=1}^{N}\exp\{i\mathbf{Q}\cdot[\mathbf{r}_j(t)-\mathbf{r}_k(0)]\}\right\rangle,\qquad(3)$$

where $\mathbf{r}_j(t)$, $j=1,\ldots,N$, is the position of the jth particle at time t.

The vector (standard) method of calculating $I(Q,t)$ [or $S(Q)$] is described in Ref. [1]. Here we note that the vector method is restricted to calculating $I(Q,t)$ at wave vector magnitudes Q that satisfy the condition $QL/2\pi=1,\sqrt{2},\sqrt{3},\sqrt{4},\ldots$, so the minimum Q value accessible by the vector method is $2\pi/L$. We shall refer to Q values that satisfy the above restriction as ''allowable'' values of Q. There is a method that can be used to approximate $I(Q,t)$ at values of $Q>2\pi/L$ which are not allowable Q values; however, as will be shown in Sec. IV, this can lead to significant errors.

The equations that describe the calculation of $I(Q,t)$ by the scalar method have been developed in a previous publication [2]. In this section we present three equations that characterize the scalar method and give a brief description of the use and limitations of these equations in calculating $I(Q,t)$. The intermediate scattering function is calculated in the scalar method by Eq. 4(a), where $u(QR)$ is defined in Ref. [2]:

$$I(Q,t)=I_N(Q,t,R)+\frac{S(0)}{N}\frac{4}{3}\pi\rho R^3 u(QR)\quad\text{for large }R,\qquad(4a)$$

where

$$I_N(Q,t,R)=4\pi\int_0^R dr\,r^2\left(\frac{\sin(Qr)}{Qr}\right)G_N(r,t)$$
$$-\frac{4}{3}\pi\rho R^3 u(QR).\qquad(4b)$$

The quantity $I_N(Q,t,R)$ is the finite system (N-particle) intermediate scattering function and, as will be seen in Appendix A, may be calculated from MD simulation results. In the calculation of $I_N(Q,t,R)$, R represents the distance from a central particle and places a limit on the extent of the calculation. The second term on the right hand side of Eq. (4a) corrects $I_N(Q,t,R)$ for finite size effects. The large R restriction on Eq. (4a) requires that the N-particle Van Hove correlation function $G_N(r,t)$ attains its asymptotic limit for $r>R$ [Eq. (31), Ref. [2]]. Hence the restriction on R in Eq. (4a) can be restated by defining $R(t)$ such that
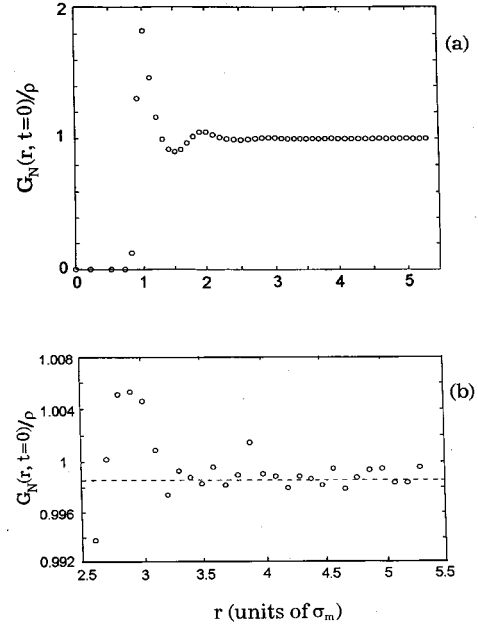

FIG. 1. Reduced N-particle Van Hove correlation function at time $t=0$, $G_N(r,0)/\rho$ vs radial distance r in units of σ_m (distance of Aziz pair potential minimum) for $N=706$. The dotted line denotes the asymptotic limit $[1-S(0)/N]$. Panels (a) and (b) highlight the first and third peaks, respectively.

$$G_N(r,t)=\rho\left[1-\frac{S(0)}{N}\right]\quad\text{for }R(t)<r<L/2.\qquad(5)$$

Thus Eqs. (4) and (5) summarize the scalar method of calculating $I(Q,t)$ and the notation $R(t)$ in Eq. (5) emphasizes the time dependence of the asymptotic region $G_N(r,t)$.

The restriction on R given by Eq. (5) has a major consequence for the calculation of $I(Q,t)$. Figures 1 and 2 show plots of $G_N(r,t)/\rho$ at $t=0$, 3.01, and 5.01 ps obtained from a 706-particle simulation, and details of the MD simulations will be given in the next section. Figure 1(a) shows the general behavior of $G_N(r,t)/\rho$ and Fig. 1(b) indicates that $G_N(r,t)/\rho$ at $t=0$ attains its asymptotic limit $1-S(0)/N$ for the range $4.0\sigma_m<r<5.39\sigma_m$, where in our case $\sigma_m=4.012$ Å and $5.39\sigma_m$ is the maximum r value accessible to a 706-particle simulation. Figure 2 demonstrates that as time increases the asymptotic region of $G_N(r,t)$ recedes to larger values of r. For example, Fig. 2(a) shows the asymptotic region beginning at $r=5\sigma_m$ for $t=3.01$ ps and Fig. 2(b) for $t=5.01$ ps indicates that the asymptotic region of $G_N(r,t)$ cannot be accessed by a 706-particle simulation. As a result, at the thermodynamic state of the simulation, we expect the scalar method applied to data from a 706-particle simulation to accurately give $I(Q,t)$ at smaller values of Q, $Q\leq 2\pi/L$, for t no larger than (roughly) 5 ps, since Eq. (5) cannot be satisfied for $t>5$ ps. For a 2048-particle system in the same thermodynamic state, an estimate of the maximum time at which the scalar approach will accurately give $I(Q,t)$ for $Q\leq 2\pi/L$ is obtained as follows. We scale the 706-particle system result $t=5$ ps by the ratio of the simulation cube edge lengths for the 2048-particle system, L
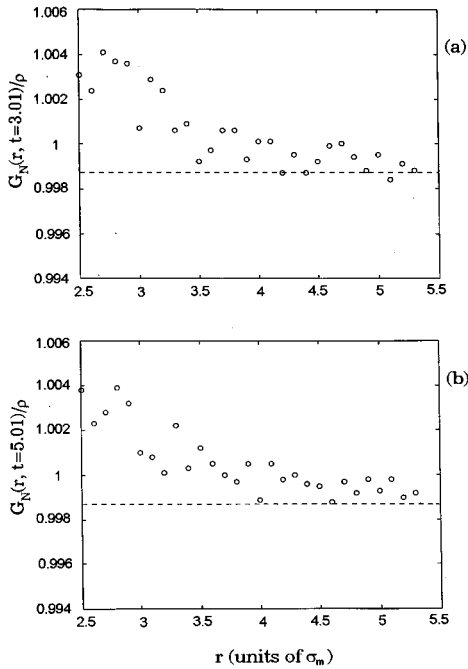
FIG. 2. Same as Fig. 1(b) except $t=3.01$ and 5.01 in panels (a) and (b), respectively.

$=15.38\sigma_m$, and 706-particle system, $L=10.78\sigma_m$, to find the new limit $t=7$ ps. Thus at roughly $t=7$ ps the asymptotic region of $G_N(r,t)$ will recede beyond the range accessible to the 2048-particle simulation; hence the scalar method will accurately give $I(Q,t)$ at smaller values of Q for t no larger than approximately 7 ps.

Perhaps a better physical understanding of the limitation imposed by Eq. (5) on the scalar method is obtained by noting that, when the asymptotic region of $G_N(r,t)$ recedes to $r>L/2$ [i.e., outside the range of validity of Eq. (4a)], it is possible that some structure would be forming in a larger (or infinite) system over the region $r>L/2$. But $I_N(Q,t,R)$ cannot account properly for this structure and thus Eq. (4a) is no longer valid. Hence, when the sphere of radius R (we assume R is roughly equal to $L/2$) associated with the calculation begins to ''leak structure,'' the scalar calculation begins to fail. As illustrated above, increasing the size (i.e., number of particles) in the simulation will allow access to larger r values and thus allow access to the asymptotic region of $G_N(r,t)$ for greater values of time; this in turn will extend the time for which Eq. (4a) is valid. We note, however, that Eq. (4a) will give spurious results only for those Q values associated with structure in the region $r>R$, or for $Q \leqslant 2\pi/L$. In addition, for this range of Q values, errors in $I(Q,t)$ will occur at smaller values of t as Q decreases. The opposite case where Q is larger than $2\pi/L$ is discussed below.

The vector method will give $I(Q,t)$ accurately for allowable values of Q and over time intervals less than the time required for a sound wave to travel L, the edge length of the simulation cube. Simulations over longer time intervals will produce errors in $I(Q,t)$ that arise from the spurious reappearance of sound waves as a result of periodic boundary conditions. However, this restriction on time associated with the vector method is much less severe than the time restriction of the scalar method for smaller Q values. For Q values that are large relative to $2\pi/L$ the scalar approach, like the vector approach, will accurately give $I(Q,t)$ with t limited only by the reappearance of sound waves. At such large Q values, the factor $\sin(Qr)/Qr$ which appears in the definition of $I(Q,t)$, $I(Q,t,R)$, and $I_N(Q,t,R)$ [Eqs. (25) and (27) of Ref. [2]] will minimize the effect on $I(Q,t)$ produced by the structure of $G_N(r,t)$ at large r. Thus $I(Q,t)$ will be unaffected as the asymptotic region of $G_N(r,t)$ changes with time.

A time expansion of $I(Q,t)$ will allow $I(Q,t)$ to be determined from simulation results for any value of Q over a limited range in t. We refer the reader to Refs. [4,6] for a general account of this method of calculating $I(Q,t)$. Here we note that our calculation of $I(Q,t)$ by this approach omits terms that contain three- and higher-particle distribution functions. The static structure factor $S(Q)$ is required by the time expansion method to calculate $I(Q,t)$, while the scalar approach requires $S(0)$ for the calculation of $I(Q,t)$. For small Q, $S(Q)$ must be obtained from an integral equation theory such as the MHNC or from the scalar approach, since the vector method of determining $S(Q)$ is inappropriate because of the $Q \geqslant 2\pi/L$ restriction. In this work the infinite system $S(Q)$ is obtained from the scalar method as described in Refs. [2,3].

III. MOLECULAR DYNAMICS SIMULATIONS

We carried out a series of MD simulations for a dense krypton fluid in which the particles interacted via the Aziz pair potential [7], characterized by the parameters $\sigma = 3.579$ Å (atomic diameter) so that $\sigma_m = 4.012$ Å (distance of potential minimum) and $T/k_B = 200$ K (well depth), with the potential truncated at a cutoff distance $r=4\sigma$. The simulation program is based on the fifth-order Gears predictor-corrector algorithm [8] that solves the classical equations of motion for particle trajectories in the microcanonical ensemble with periodic boundary conditions. The simulations were performed for two system sizes $N=706$ and 2048 in a thermodynamic state defined by the reduced temperature $T^*=k_BT/\varepsilon=1.508$ and reduced density $\rho^*=\rho\sigma^3=0.40$. (For comparison, the critical point of krypton occurs at $T^* = 1.05$, $\rho^*=0.3$.) The system state closely approximates the state used in a previous publication [3] in which $S(Q)$ was calculated. The relatively large compressibility associated with this thermodynamic state makes it ideal to illustrate the scalar approach to calculating both $S(Q)$ and $I(Q,t)$. For the 706- and 2048-particle systems nine independent simulations were performed with each simulation consisting of 2×10^5 time steps.

The 706-particle simulation has an edge length $L=10.78\sigma_m$, and the allowable Q values associated with the vector method of calculating $I(Q,t)$ are given by $Q\sigma_m = 0.583$, 0.823, 1.01, and 1.166, . . . , with the number of noncolinear vectors **Q** associated with each allowable value being 3, 6, 4, and 3, respectively. Please note that for a given value of Q there are essentially an infinite number of non-

collinear vectors $\mathbf{Q}$ for which $|\mathbf{Q}|=Q$. However, the use of periodic boundary conditions in the simulation requires that the $\mathbf{Q}$ vectors satisfy the restriction $\mathbf{Q}=(2\pi/L)(k_1,k_2,k_3)$, where $k_i=0,\pm 1,\pm 2,\ldots$, with $i=1,2,3$. This restriction gives rise to the relatively small number of noncollinear vectors $\mathbf{Q}$ associated with the allowable values of Q in the vector calculation. To obtain $I(Q,t)$ for $Q>0$ by the scalar method, R values of $4.5\sigma_m$ and $5.0\sigma_m$ were used in the right hand side (RHS) of Eq. (4a) and the results were then averaged to obtain $I(Q,t)$. The technique of averaging over values of R was employed to obtain a representative value of the quantity $I_N(Q,t,R)$ of Eq. (4) for R in the asymptotic region of $G_N(r,t)$. Averaging over R values produces a modest decrease in the fluctuations of $I(Q,t)$. Finally, $S(0)=0.91 \pm 0.06$ was calculated via Eq. (23) of Ref. [2] for the $N =706$ case.

In the 2048-particle simulation $L=15.37\sigma_m$, the allowable Q values are given by $Q\sigma_m=0.409$, 0.578, 0.708, and $0.816,\ldots$, and the number of noncolinear vectors $\mathbf{Q}$ are 3, 6, 4, and 3, respectively. In the scalar method, R values of $7.0\sigma_m$ and $7.5\sigma_m$ were used in the RHS of Eq. (4a) and the results averaged to give $I(Q,t)$. Use of Eq. (23) of Ref. [2] gave a value of $S(0)=0.90\pm 0.08$. Note that the values obtained for $S(0)$ agree with the results of our previous work with colleagues [3]. Obtaining $I(Q,t)$ by averaging R may average out fluctuations in $I(Q,t)$, which suggests that one should use a single R value in the velocity of sound calculations. This is because anomalies (fluctuations) in $I(Q,t)$ will be used in Sec. V to determine the velocity of sound in our simulations. Therefore in calculating the $Q=0$ data, $I(Q,t)$ was obtained by the scalar method using a single R value of $5.38\sigma_m$ in the $N=706$ case and a single R value of $7.5\sigma_m$ in the $N=2048$ case.

During the simulation, configurations (particle coordinates) were periodically saved and subsequently analyzed to determine $I(Q,t)$. In Appendix A we describe the scalar method and the vector method of obtaining $I(Q,t)$. For both the 706- and 2048-particle simulations, coordinates were stored every 1.0023 ps, implying that $I(Q,t)$ can be obtained for $t=1.0023n$ ps, $n=1,2,3,\ldots$. The quantity $I_N(Q,t,R)$ is a measure of the degree of correlation between particle configurations separated by time t as noted in Ref. [3]. This property of $I_N(Q,t,R)$ is used to ensure the independence of the estimates $X_k(Q,t)$ used in Eq. (A2) below to obtain $X(Q,t,M)$. Separating successive reference coordinate sets used in the calculation of $X_k(Q,t)$ by a time interval t large enough to ensure that $I_N(Q,t,R)=0$ implies that the reference coordinate sets are uncorrelated and hence that X_k's are independent. Note that independence of the X_k's is necessary for σ_M, or the error in Eq. (A4), to be calculated by Eq. (A3). In calculating $I(Q,t)$ from the 706-particle simulation data, reference coordinates were separated by a fixed time interval of 30 ps plus a random interval between 0 and 10 ps giving an average separation of 35 ps. The quantity $I_N(Q,t,R)$ decays more slowly as the system size increases; hence the 2048-particle system required a separation consisting of a fixed interval of 50 ps plus a random interval of between 0 and 20 ps implying an average separation of 60
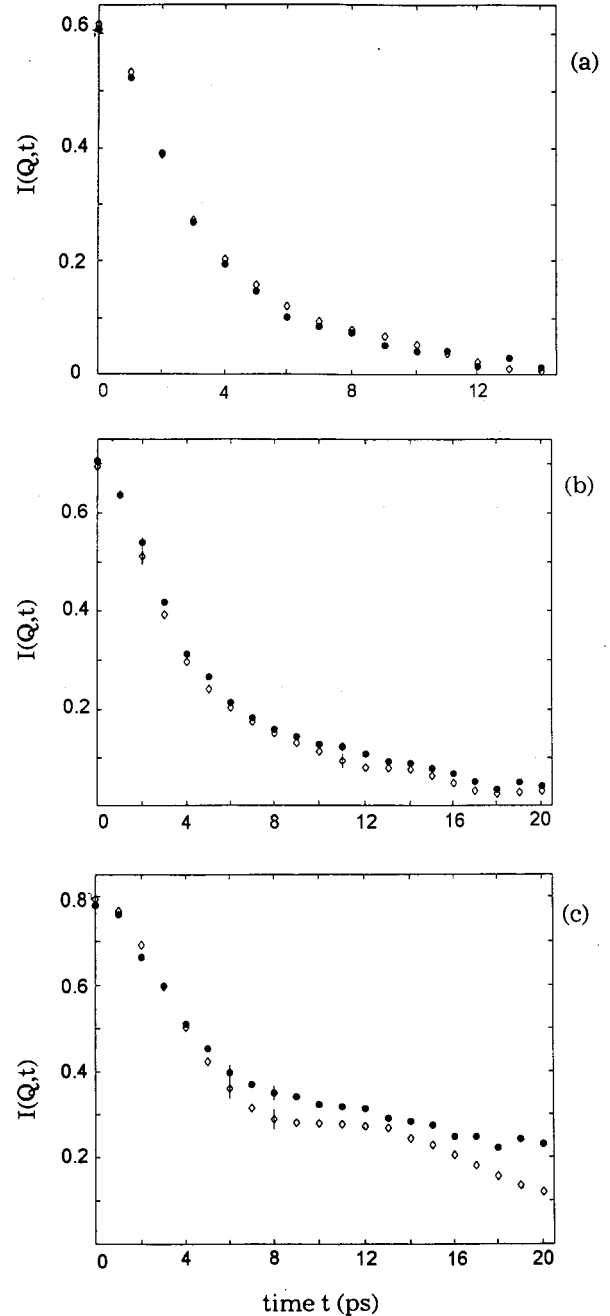

FIG. 3. Intermediate scattering function $I(Q,t)$ determined by the scalar method (shaded circles) and vector method (diamonds) applied to 706-particle MD data vs time t: $Q\sigma_m$ (a) 1.01, (b) 0.823, (c) 0.583. The vertical lines in panels (b) and (c) at selected values of t represent error bars.

ps. The time separating successive reference coordinates contained a random component to further ensure the independence of the estimates $X_k(Q,t)$.

IV. RESULTS AND ANALYSIS OF $I(Q,T)$ CALCULATIONS

Figure 3 illustrates $I(Q,t)$ obtained by the scalar method (circles) and the vector method (diamonds) from the 706-

FIG. 4. Intermediate scattering function $I(Q,t)$ determined by the scalar method (circles) applied to 706-particle MD data and vector method (diamonds) applied to 2048-particle MD data for $Q\sigma_m=0.708$. Also shown is $I(Q,t)$ obtained from the vector method applied to 706-particle MD data by averaging over ''allowable'' Q values (stars).
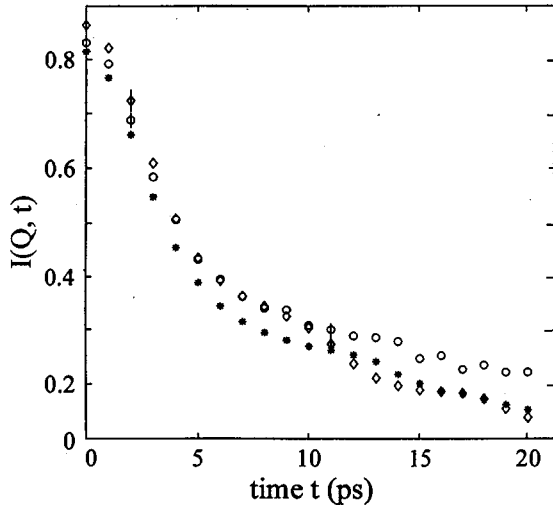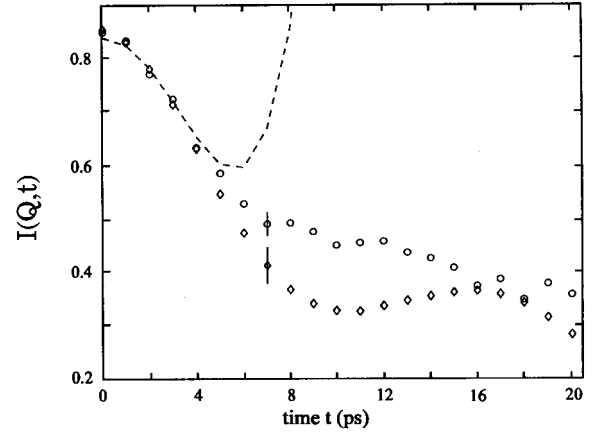

FIG. 5. Intermediate scattering function $I(Q,t)$ determined by the scalar method (circles) applied to 706-particle MD data and vector method (diamonds) applied to 2048-particle MD data vs time t for $Q\sigma_m=0.409$. Also shown is $I(Q,t)$ determined by the time expansion approach (dotted line).

particle simulation results for $Q\sigma_m=1.01$, 0.823, and 0.583. At selected values of t, vertical lines centered on a circle (diamond) of total length $2\delta_M$ ($2\tilde{\delta}_M$) represent the error associated with the scalar (vector) method. Note that both δ_M and $\tilde{\delta}_M$ are modestly time dependent with the uncertainty slightly larger at smaller values of time. Fig. 3(c) shows that for $Q\sigma_m=0.583$ the results of the scalar and vector methods begin to diverge for $t>6$ ps. As noted above, this divergence is due to spurious results of the scalar method caused by the deterioration of the asymptotic region of $G_N(r,t)$. This should be compared to our estimate that the 706-particle scalar result would be valid for t no larger than 5 ps. As Q increases, the effect on $I(Q,t)$ caused by the structure of $G_N(r,t)$, for large r, decreases and thus for $Q\sigma_m=0.823$ and 1.01 the scalar and vector methods agree nicely. Note, however, that there is a modest disagreement between these methods for $Q\sigma_m=0.823$ at $t=11$ and 12 ps, which we feel is due to the greater effect of sound waves as a result of periodic boundary conditions. We discuss this matter further in Sec. V.

Figure 4 compares $I(Q,t)$ for $Q\sigma_m=0.708$ obtained from the 2048-particle vector calculation (diamonds), 706-particle scalar calculation (circles), and 706-particle vector calculation (stars). The 706 scalar results and the 2048 vector results start to disagree for $t\geq12$ ps due to the effect of sound waves in the smaller system, hence the scalar result is in error for $t\geq12$ ps. Note that $Q\sigma_m=0.708$ is not an allowable Q value associated with a 706-particle vector calculation, and the $I(Q,t)$ shown in Fig. 4 (stars) was obtained as an average over $I(Q,t)$ for $Q\sigma_m=0.583$ and 0.823. This averaging technique is a standard approach used to obtain $I(Q,t)$ for nonallowable Q values by the vector method and, as shown in Fig. 4, can lead to significant errors. Finally, note the modest ''hump'' in the 706 vector results for t between 11 and 14 ps,

which suggests the reappearance of a sound wave in the 706-particle system at approximately 11 ps.

Figure 5 compares $I(Q,t)$ for $Q\sigma_m=0.409$ obtained by the scalar method using the 706-particle simulation results (circles), by the vector method using the 2048-particle simulation results (diamonds), and by the time expansion approach (dashed line). We note that the vector method could not have been applied to the 706-particle MD data for $Q\sigma_m<0.583$. For $t>6$ ps the results of the scalar and vector methods begin to disagree because of errors in the scalar approach caused by the deterioration of the asymptotic region of $G_N(r,t)$ contained within the 706-particle system. The shape of the dashed line indicates that the time expansion results are in error for $t>5$ ps. $Q\sigma_m<0.409$ the vector method cannot be applied to the 2048-particle MD results. Comparisons between the 2048-particle scalar results (circles), 706-particle scalar results (stars), and time expansion results (dashed line) are illustrated in Fig. 6 for $Q\sigma_m=0.30$. All results shown agree to within error bars for $t\leq4$ ps. The time expansion results are in error for $t\geq7$ ps as evidenced by the shape of the curve depicting these results. The 706-particle scalar results disagree with the 2048-particle scalar results and the expansion results at $t=5$ ps, suggesting that the 706-particle scalar results are in error for times $t>5$ ps.

The following scaling argument suggests that the 2048-particle scalar results are correct for $t\leq9$ ps in the $Q=0.30$ case. We recall that the scalar method accurately gives $I(Q,t)$, with $Q\sigma_m=0.409$, for $t\leq6$ ps in the 706-particle case (see Fig. 5). But $Q\sigma_m=0.409$ relative to a 706-particle system implies a smaller quantity than $Q\sigma_m=0.3$ relative to a 2048-particle system [since the quantity QL is smaller for $Q\sigma_m=0.409$ and $L=10.78\sigma_m$ (706-particle system) than for $Q\sigma_m=0.30$ and $L=15.37\sigma_m$ (2048-particle system)] implying that the 2048-particle scalar results are correct for $t\leq9$ ps.

Figure 7 illustrates $I(Q,t)$ (circles) and $S(Q)$ (dashed line) for $Q=0$ with both quantities obtained by the scalar
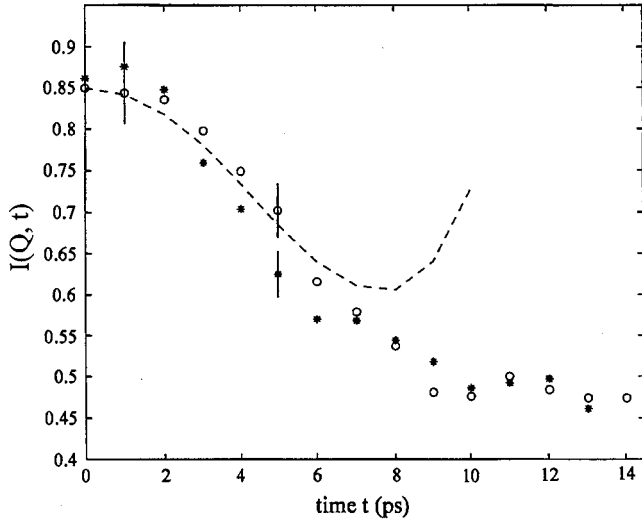
FIG. 6. Intermediate scattering function $I(Q,t)$ determined by the scalar method applied to MD data from a 706-particle system (stars), 2048-particle system (circles), and the time expansion approach (dotted line) vs time t for $Q\sigma_m = 0.30$.

method [$S(0)$ determined by Eq. (23) of Ref. [2]]. For $Q = 0.0$, $I(Q,t) = S(Q)$ for all values of t. Also, as shown in Fig. 7(a), the 706-particle results for $I(Q,t)$ are correct (within the fluctuations) for $t \leqslant 3$ ps and, as shown in Fig. 7(b), the 2048-particle results are correct for $t \leqslant 5$ ps.

We now consider the accuracy and efficiency of the scalar and vector methods for calculating $I(Q,t)$. The uncertainties (standard deviation) in $I(Q,t)$ associated with the scalar calculation and the vector calculation are denoted by δ_M and $\tilde{\delta}_M$, respectively, and both of these quantities are inversely proportional to $\sqrt{M}$, where M is the number of estimates used to obtain $I(Q,t)$. Also, for a given value of Q, M had a common value in the scalar and vector calculations reported in this work. We shall compare the conditions under which the uncertainties in these methods are equal.

In the $N = 706$, $Q\sigma_m = 1.01$ case [Fig. 3(a)] $\tilde{\delta}_M / \delta_M > 2$ at all values of time with the time averaged values of $\tilde{\delta}_M$ and δ_M being 0.016 and 0.007, respectively. Hence the number of estimates in the vector calculation must be increased by a factor of (at least) 4 in order to reduce the uncertainty of the vector approach to that of the scalar approach. This in turn would require extending the length of the MD simulations by a factor of 4. The scalar calculation of an estimate of $I(Q,t)$ requires the evaluation of a sum containing N^2 terms [Eq. (A1a) below], while the vector calculation of an estimate requires the evaluation of four summations, each containing N terms [Eq. (A5)], therefore the vector approach is the more efficient method of calculating a single estimate of $I(Q,t)$. However, because of the increased number of estimates required by the vector approach, the scalar approach is a much more efficient method of calculating $I(Q,t)$ for $Q\sigma_m = 1.01$ at a given uncertainty. In particular, the 706-particle MD simulations were run on an IBM RS/6000 computer workstation and required a total of 570 h to complete. Analyzing the data to obtain $I(Q,t)$ for $Q\sigma_m = 1.01$ required roughly 4 min of computer time in the vector calculation, while the
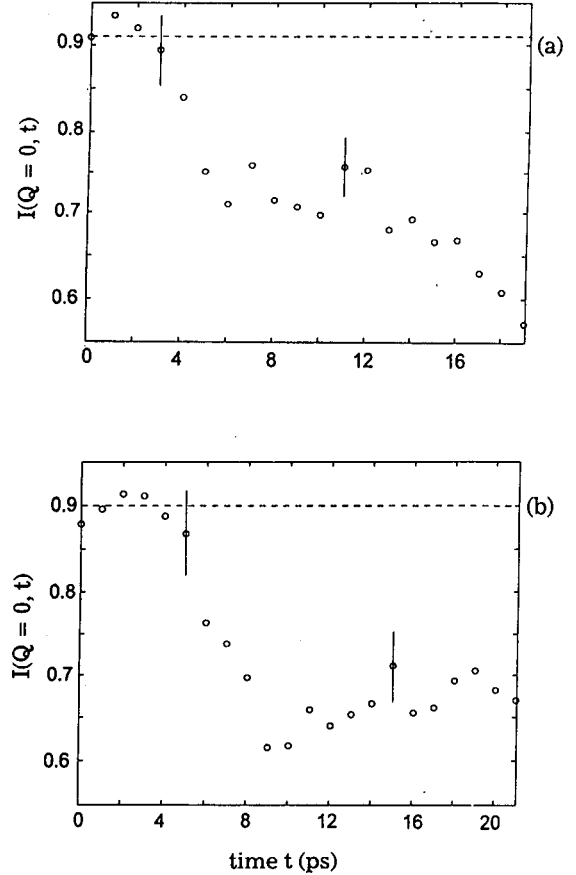

FIG. 7. Intermediate scattering function $I(Q,t)$ (circles) and the static structure factor $S(Q)$ (dotted line) for $Q = 0.0$ obtained by the scalar method. Panel (a) shows results associated with the 706-particle MD data, and panel (b) illustrates the 2048-particle results.

scalar calculation required 2 h. However, as previously noted, to reduce the uncertainty of the vector results to those of the scalar results would necessitate quadrupling the data set, an effort that would require approximately 2280 h of computer time. Thus overall the scalar calculation is more efficient, requiring roughly 572 h of computing compared to 2280 h required for the vector calculation.

The scalar method has a similar advantage in calculating $I(Q,t)$ for $N = 706$ in the $Q\sigma_m = 0.823$ and $Q\sigma_m = 0.583$ cases with $\tilde{\delta}_M / \delta_M > 1.5$ for all values of time in each case. The time averaged values of $\tilde{\delta}_M$ and δ_M are 0.015 and 0.010 in the $Q\sigma_m = 0.823$ case and 0.026 and 0.018 in the $Q\sigma_m = 0.583$ case. A relatively large uncertainty in the vector calculation results from the small number of $\mathbf{Q}$ vectors which can be used in Eq. (A5) below to obtain an estimate of $I(Q,t)$. For example, as noted in Sec. III there are a total of three $\mathbf{Q}$ vectors that can be used to obtain $I(Q,t)$ for $Q\sigma_m = 0.409$. Increasing the value of Q generally increases the number of $\mathbf{Q}$ vectors available for calculating $I(Q,t)$ by the vector method. In the $Q\sigma_m = 3.14$ case there is a total of 36 such $\mathbf{Q}$ vectors. Use of all 36 vectors yields an average uncertainty in $I(Q,t)$ of 0.003; however, using only four of the 36 $\mathbf{Q}$ vectors increases the average uncertainty to a value of 0.01. The scalar method of calculating $I(Q,t)$ for $Q\sigma_m$
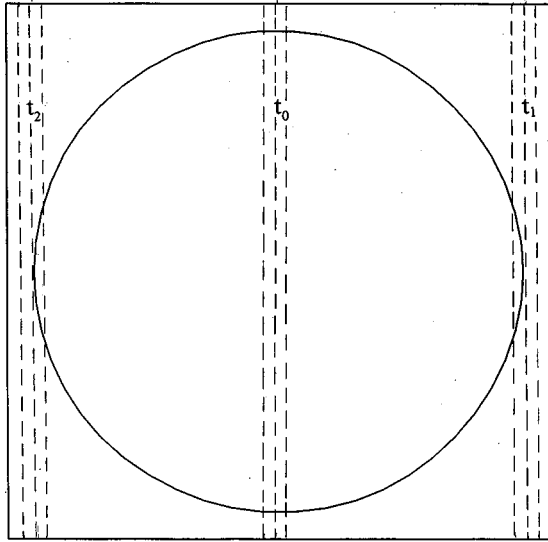
FIG. 8. Cross section of the primary simulation cube. The circle represents the cross section of the sphere of radius R used in Eq. (A1) below to calculate $X_k(Q,t)$. The dotted lines represent the crest of a sound wave as it moves through the simulation cube and is initially positioned at the cube's center at time t_0, moves to the right end of the cube at t_1, and, due to the effect of periodic boundary conditions, occupies the left end of the cube at t_2, where $t_0 < t_1 < t_2$.

$=3.14$ produces an average uncertainty of 0.001. Hence, even in a case where the vector method has access to a relatively large number of **Q** vectors, the scalar method is the more efficient method of calculating $I(Q,t)$ at a given uncertainty.

The source of the difference in efficiency of the scalar and vector calculations can be understood by noting that Eq. (25) of Ref. [2], a basic equation of the scalar method, can be obtained by averaging (integrating) Eq. (1) over all **Q** vectors with a fixed magnitude of Q. Consequently, the scalar method averages over an essentially infinite number of **Q** vectors and the vector method averages over a finite number of **Q** vectors. As a result the scalar calculation of $I(Q,t)$ has a smaller uncertainty than the vector calculation.

V. VELOCITY OF SOUND

We begin by reviewing the behavior of $I(Q=0,t)$. As $t \rightarrow 0$, $I(Q=0,t)$ becomes $S(Q=0)$ which as a value of 0.91 in the $N=706$ case. At higher t Fig. 7(a) shows that $I(Q=0,t)$ has a local maximum at (roughly) 11.5 ps. We recall that other anomalies in the behavior of $I(Q,t)$ were illustrated in Figs. 3(b) and 4, occurring at approximately 11 and 12 ps, respectively, and were attributed to the effect of sound waves. Similarly, we shall attribute the aforementioned behavior of $I(0,t)$ to the effect of sound waves, an effect which we now discuss in some detail.

Figure 8 shows the cross section of the primary simulation cube and the dashed lines denote the crest of a sound wave at various points in time as the wave moves in the x direction through the cube. As time increases through values $t_0 < t_1 < t_2$ the crest of the wave moves from the center of the

figure to the right end of the cube and, due to periodic boundary conditions, appears at the left end of the cube at time t_2. The crest will continue to move to the right and at some point in time overlap with its initial position at time t_0; hence the wave will have traversed the whole simulation cube. The circle represents the cross section of the sphere of radius R used in Eq. (A1) below to calculate $X_k(Q,t)$, where the ith particle associated with Eq. (A1a) is assumed for simplicity to be at the cube's center. In terms of the notation of Eq. (A1a), $t_0 \equiv t_k$ and the position of the ith particle is denoted as $r_i(t_0)$. Figure 8 indicates that as the wave moves toward the right end of the cube the sphere contains less of the crest or dense part of the wave and hence the number of particles contained in the sphere decreases. The sphere will continue to lose particles until the crest, due to periodic boundary conditions, reenters the left end of the sphere. At this point the number of particles within the sphere will start to increase and will reach a maximum when the wave's crest reaches its initial position—when the wave has traveled the length of the simulation cube.

For $Q=0$ the sum over j in Eq. (A1a) counts the number of particles contained in the sphere of radius R at time $t_0 + t$, given that there existed a particle at the sphere's center (ith particle) at time t_0. Hence the values of $X_k(0,t)$, $I_N(0,t,R)$, and $I(0,t)$ [Eqs. (A1a) and (4)] will be affected by the position of the sound wave, and in particular $I(0,t)$ will register an increase in value and exhibit a local maximum at the time t required for a sound wave to travel the length of the simulation cube. In the above discussion we have focused on one central (ith) particle contained within the crest of a sound wave traveling in the x direction. However, it should be noted that each particle contained within the wave's crest at time t_0 (Fig. 8), when used as the ith particle in Eq. (A1a), will effect an increase in $I(0,t)$ at the time t required for the wave to travel the length of the simulation cube.

Figure 7(a) shows the average $I(Q,t)$ obtained from nine independent simulations. The local maximum that occurs in the vicinity of 11.5 ps indicates that a sound wave requires roughly 11.5 ps to traverse the length of the simulation cube. We have analyzed the results of the independent simulations used to obtain Fig. 7(a) and have obtained the location in time of the maximum value of $I(Q,t)$ in the vicinity of 11.5 ps for each of the nine simulations. This analysis yields nine values ranging from 11.02 to 14.03 ps with an average value and standard deviation of 11.8 and 1.0 ps, respectively. Hence we have determined that a sound wave requires 11.8 ± 1.0 ps to traverse the simulation cube, and this corresponds to a velocity of sound in the 706-particle simulation of 366 ± 34 m/s. In the 2048-particle case, analyzing each of the nine simulations associated with Fig. 7(b) indicates that a sound wave requires 17.6 ± 2.9 ps to travel the length of the simulation cube, and this corresponds to a velocity of sound of 350 ± 58 m/s. These are finite system results, which are size dependent. When going to an infinite system we expect the velocity of sound to have a modestly smaller value since the compressibility will be larger for the infinite system.

Experimental results [9] give the velocity of sound in krypton at 300 K for densities of 7.94 and 8.96 atoms/nm^3 as

TABLE I. Velocity of sound (m/s) for krypton gas at $\rho = 8.725$ atoms/nm^3 and $T = 301.6$ K.

Experimental results	
With many-body forces (observed)	335.5
Subtracting calculated effect of many-body forces	317
Scalar MD simulation results	
$N = 706$ case	366 ± 34
$N = 2048$ case	350 ± 58

307.41 and 343.15 m/s, respectively. Linearly interpolating between these results yields an estimate of the velocity of sound in bulk krypton of 335.5 m/s at the simulation density of 8.725 atoms/nm^3 ($\rho^* = 0.40$) and the simulation temperature of $T = 301.6$ K ($T^* = 1.508$). The velocity of sound data are listed in Table I.

When comparing the experimental sound velocity with the results obtained from the 706- and 2048-particle MD simulations, many-body forces and size effects must be considered. In Appendix B we obtain a value of 317 m/s as a rough estimate of the velocity of sound in bulk krypton at the simulation density and pressure with many-body effects removed. We stress that, because our simulations do not account for many-body effects, these effects must be subtracted from the experimental results to obtain a valid comparison of experimental and simulation results of the velocity of sound. Table I shows that the experimental velocity of sound result with many-body effects removed falls within the lower limit of the 2048-particle simulation result and is slightly below the lower limit of the 706-particle simulation result. However, as we argue in Appendix B, the sound velocity in an N-particle simulation decreases as N increases. Because of this, our 706- and 2048-simulation results for the velocity of sound must be reduced before comparing them to experimental results that refer to bulk krypton (infinite-N case). An estimate of the magnitude of the reduction that must be applied to the N-particle simulation results was not obtained since this would have required a substantial amount of computer time. Here we simply note that reducing the simulation results by roughly 10% brings the simulation and experimental results into essentially perfect agreement.

VI. SUMMARY AND CONCLUSIONS

We have applied a method for obtaining low momentum transfer data on fluids from a computer simulation. While our earlier work with colleagues [2,3] concentrated on the equal time correlation functions at low momentum transfer, we have extended these methods to the finite time correlation functions. Data were obtained for a kryptonlike fluid pair potential at a state above the critical point, and good agreement between this method and other data was obtained. In particular, we have concentrated on the intermediate scattering function $I(Q,t)$ at low t and on the velocity of sound for this state. We have shown how data obtained with existing MD methods may be extended using our method. Both the most useful procedures and the limitations of our approach have been investigated. For example, we have shown how the calculation of $I(Q,t)$ at smaller values of Q is affected as

the asymptotic region of $G_N(r,t)$ recedes to larger r as t increases.

Also, we compared MD results obtained by the vector and scalar methods, and showed how the range of time over which the two sets of data agreed varies with the value of $Q\sigma_m$. Then we compared scalar results for a 706-particle system with vector method results for a larger 2048-particle system. These results showed the complementarity of the two methods. We also compared these results to those obtained by a short collision time expansion (Figs. 5 and 6) and demonstrated the usefulness and the limits to this expansion. The fact that the scalar method described here gives valid results for low t in the limit $Q \rightarrow 0$ was illustrated by the data presented in Fig. 7. In addition, we compared the efficiency of the scalar and vector approaches and found that for the cases in which $I(Q,t)$ was calculated by both methods the scalar method was significantly more efficient at a given level of uncertainty. Finally, we deduced the velocity of sound in our system from the anomalous behavior of $I(Q = 0, t)$ as t was increased. It compared well to the value deduced from experimental data on real krypton after correcting for the three-body potential term.

Thus we have tested the scalar method in a number of ways and a variety of conditions. Its usefulness in extending MD data on finite systems to smaller values of Q over a restricted range of t has been demonstrated. We hope this will lead to its use in a variety of calculations.

APPENDIX A: CALCULATION OF $I(Q,t)$ IN A MD SIMULATION

We first describe how to obtain $I(Q,t)$ via the scalar method. Consider a pair of coordinate sets separated in time by time interval t. One coordinate set, referred to as the reference set, contains particle positions $r_i(t_k)$, $i = 1, \ldots, N$, and the other coordinate set, referred to as the correlation set, contains positions $r_j(t_k + t)$, $j = 1, \ldots, N$. From the reference set a particle i is arbitrarily selected and all particles j of the correlation set contained within a sphere of radius R with center $r_i(t_k)$ are determined. The factor $[\sin(Qr_{ij})/Qr_{ij}]$, r_{ij} being the distance between particles i and j, is summed over all j. Next another particle i is chosen, the same sum is calculated, and the process is repeated until every reference particle has served as a central particle. The average over all $i = 1, \ldots, N$ of the calculated sums represents a single estimate of the integral in Eq. (4b) that defines $I_N(Q,t,R)$. This estimate, which we denote as $X_k(Q,t)$, is expressed analytically as

$$X_k(Q,t) = \frac{1}{N} \sum_{i=1}^{N} \sum_{j=1}^{N} \left\{ \frac{\sin[Qr_{ij}(t_k,t)]}{Qr_{ij}(t_k,t)} \right\} \Delta_{ijk}(t,R),$$

(A1a)

where

$$\Delta_{ijk}(t,R) = \begin{cases} 1 & \text{if } r_{ij}(t_k,t) \leq R, \\ 0 & \text{if } r_{ij}(t_k,t) > R \end{cases}$$

(A1b)

and $r_{ij}(t_k,t) = |\mathbf{r}_i(t_k) - \mathbf{r}_j(t_k+t)|$ is defined as the minimum distance between particles i at time t_k and either particle j or its nearest periodic image at time t_k+t.

Averaging M independent estimates $X_k(Q,t)$ obtained from M independent reference sets gives the following approximation to the integral in Eq. (4b):

$$X(Q,t,M) = \frac{1}{M} \sum_{k=1}^{M} X_k(Q,t).$$

(A2)

The variance in $X(Q,t,M)$ may be approximated by

$$\delta_M^2 = \frac{1}{M^2} \sum_{k=1}^{M} [X_k(Q,t) - X(Q,t,M)]^2$$

(A3)

and the standard deviation δ_M represents the uncertainty in $\mathcal{X}(Q,t,M)$. Hence the integral in Eq. (4b) may be approximated by $X(Q,t,M) \pm \delta_M$ and

$$I_N(Q,t,R) = X(Q,t,M) - \frac{4}{3} \pi \rho R^3 u(QR) \pm \delta_M.$$

(A4)

Equation (A4) is used to obtain $I_N(Q,t,R)$ from simulation data, which when substituted into Eq. (4) at sufficiently large R leads to the scalar approximation of $I(Q,t)$ for arbitrary Q.

The vector method of calculating $I(Q,t)$ requires the evaluation of the ensemble average of Eq. (3) which is obtained from a MD simulation as follows. A reference set of coordinates and a correlation set of coordinates give $r_j(t_k)$, $j=1,\ldots,N$, and $r_j(t_k+t)$, $j=1,\ldots,N$, respectively, from which an estimate of $I(Q,t)$, denoted by $Y_k(Q,t)$, is determined via

$$Y_k(Q,t) = \frac{1}{m} \sum_{i=1}^{m} \frac{1}{N} \left\{ \left[\left(\sum_{j=1}^{N} \cos[\mathbf{Q}_i \cdot \mathbf{r}_j(t_k)] \right) \right. \right.$$

$$\times \left(\sum_{j=1}^{N} \cos[\mathbf{Q}_i \cdot \mathbf{r}_j(t_k+t)] \right)$$

$$+ \left(\sum_{j=1}^{N} \sin[\mathbf{Q}_i \cdot \mathbf{r}_j(t_k)] \right)$$

$$\left. \left. \times \left(\sum_{j=1}^{N} \sin[\mathbf{Q}_i \cdot \mathbf{r}_j(t_k+t)] \right) \right] \right\}.$$

(A5)

The quantity in the brackets $\{\cdots\}$ represents an estimate of $I(\mathbf{Q},t)$ and follows from Eq. (3) by factoring the complex exponential, expressing each factor in its equivalent sine-cosine form, and noting that $I(\mathbf{Q},t)$ is a real function for

classical fluids. The vector $\mathbf{Q}$ has magnitude $|\mathbf{Q}| = Q$, and averaging over a set of m such vectors yields a single estimate of $I(Q,t)$ given by Eq. (A5). Then the $Y_k(Q,t)$ obtained from M independent (uncorrelated) reference sets yields the following approximation for $I(Q,t)$:

$$I(Q,t) = \frac{1}{M} \sum_{k=1}^{M} Y_k(Q,t) \pm \tilde{\delta}_M$$

(A6)

where $\tilde{\delta}_M$ is the standard deviation associated with the average of the Y_k's [see Eq. (A3)].

APPENDIX B: VELOCITY OF SOUND; MANY-BODY FORCES AND SIZE EFFECTS

We first consider how many-body forces influence the velocity of sound. Figure 5 of Ref. [10] compares plots of $P/\rho kT$ vs ρ for $T=297$ K obtained from Monte Carlo simulations using pair interactions and obtained from experimental results. At the simulation density $\rho=8.725$ atoms/nm^3, the simulation pressure is significantly below the experimental pressure. A decrease in pressure produces a decrease in density, which in turn implies a decrease in the velocity of sound in bulk krypton as seen by comparing the velocity of sound results of Ref. [9] that were given in Sec. V. Hence ''removing'' many-body effects reduces the speed of sound at the state point of interest.

It follows that the estimate of the velocity of sound in bulk krypton of 335.5 m/s must be reduced (many-body effects removed) before comparing it to the MD simulation results. It is difficult to precisely estimate the size of the reduction. However, a rough estimate can be obtained by calculating the sound velocity in bulk krypton at the simulation pressure, which as noted above will correspond to a reduced density. The MD simulations produced a pressure of 263 atm, which the results of Ref. [9] show to be approximately 10% below the pressure of bulk krypton at the simulation temperature and density. Linearly interpolating between the experimental results in Ref. [9] shows that a pressure of 263 atm corresponds to a density of 8.18 atoms/nm^3 and a sound velocity of 317 m/s. Note that 317 m/s is our estimate of the velocity of sound in bulk krypton at the simulation density and temperature with the many-body effects removed.

We now consider the influence of size effects on the velocity of sound obtained from our simulation results. Here we give a qualitative argument that the velocity of sound will decrease as the system size become infinite. The isothermal compressibility K_T is related to the static structure factor $S(Q)$ at $Q=0$ by [4,5]

$$K_T = S(0) K_T^0,$$

(B1)

where K_T^0 is the ideal gas compressibility. Consider the system depicted in Fig. 8: a primary simulation cube containing a sphere of radius R with N representing the total number of particles in the cube and N_R representing the number of particles contained within the sphere. Let $N \to$ infinite, while R remains constant; hence the walls of the simulation cube in

Fig. 8 will recede to infinity. In the infinite-N case, $S(0)$ is equal to the fluctuations per particle of the particles contained in the sphere [4,5]; thus

$$S(0) = \frac{\langle N_R^2 \rangle - \langle N_R \rangle^2}{\langle N_R \rangle}. \quad \text{(B2)}$$

The validity of Eq. (B2) requires that R be large enough so that the average number of particles contained within a sphere of radius R, $\langle N_R \rangle$, be statistically well defined. In our calculation the value of R ranged between $4.5\sigma_m$ and $7.5\sigma_m$ which corresponds to a value of $\langle N_R \rangle$ between 215 and 996.

Now consider the finite-N case and imagine a particle contained within the sphere near the right boundary of the simulation cube (see Fig. 8). Assume the particle moves to the right and exits the sphere and simulation cube and, because of periodic boundary conditions, the particle's image reenters the left boundary of the sphere. This type of correlated motion reduces the fluctuations in the number of particles contained in the sphere as compared to the infinite-N case. Hence, for a finite system, periodic boundary conditions somewhat reduce the size of the right hand side of Eq. (B2). Therefore if we assume that Eqs. (B1) and (B2) can be used to define the finite system isothermal compressibility K_T^N, then K_T^N will be an increasing function of N. The ratio of the adiabatic compressibility K_s to K_T is equal to the ratio of the isobaric and isometric heat capacities, and, assuming this applies to the finite system case, K_s^N is also an increasing function of N. Also, in the infinite-N case, the velocity of sound is inversely proportional to the square root of K_s [8]. If we assume that this relationship holds in the finite-N case, then the velocity of sound will be inversely proportional to K_s^N and the velocity of sound will decrease as N increases. Hence our simulation results for the velocity of sound must be reduced before comparing them to experimental results.

[1] D. C. Rapaport, *The Art of Molecular Dynamic Simulation* (Cambridge University Press, Cambridge, 1995).

[2] J. J. Salacuse, A. R. Denton, and P. A. Egelstaff, Phys. Rev. E **53**, 2382 (1996).

[3] J. J. Salacuse, A. R. Denton, P. A. Egelstaff, M. Tau, and L. Reatto, Phys. Rev. E **53**, 2390 (1996).

[4] P. A. Egelstaff, *An Introduction to the Liquid State*, 2nd ed. (Oxford University Press, New York, 1992).

[5] J. P. Hansen and I. R. McDonald, *Theory of Simple Liquids* (Academic, New York, 1976).

[6] J. P. Boon and S. Yip, *Molecular Hydrodynamics* (McGraw-Hill, New York, 1980).

[7] R. A. Aziz, Mol. Phys. **38**, 177 (1979).

[8] J. M. Haile, *Molecular Dynamics Simulation* (Wiley, New York, 1992).

[9] J. Juza and O. Sifner, Acta Tech. CSAV **21**, 1 (1976).

[10] J. Ram and P. A. Egelstaff, Phys. Chem. Liq. **84**, 29 (1984).